Upgrade of goniospectrophotometer GEFE for near–field scattering and fluorescence radiance measurements

Berta Bernad, Alejandro Ferrero, Alicia Pons, M. Luisa Hernanz and Joaquín Campos

Instituto de Óptica, Agencia Estatal Consejo Superior de Investigaciones Científicas, c/Serrano 144, Madrid 28006, Spain

ABSTRACT

The goniospectrophotometer GEFE, designed and developed at IO–CSIC (*Instituto de Óptica, Agencia Estatal Consejo Superior de Investigaciones Científicas*), was conceived to measure the spectral Bidirectional Reflectance Distribution Function (BRDF) at any pair of irradiation and detection directions. Although the potential of this instrument has largely been proved, it still required to be upgraded to deal with some important scattering features for the assessment of the appearance. Since it was not provided with a detector with spatial resolution, it simply could not measure spectrophotometric quantites to characterize texture through the Bidirectional Texture Function (BTF) or translucency through the more complex Bidirectional Scattering–Surface Reflectance Distribution Function (BSSRDF). Another requirement in the GEFE upgrading was to provide it with the capability of measuring fluorescence at different geometries, since some of the new pigments used in industry are fluorescent, which can have a non–negligible impact in the color of the product. Then, spectral resolution at irradiation and detection had to be available in GEFE. This paper describes the upgrading of the goniospectrophotometer GEFE, and its new capabilities through the presentation of sparkle and goniofluorescence measurements. In addition, the potential of the instrument to evaluate translucency by the measurement of the BSSRDF is briefly discussed.

Keywords: Goniospectrophotometry, BSSRDF, BRDF, fluorescence, sparkle, translucency, appearance

1. INTRODUCTION

In last years, the measurement of appearance of objects has gained increasing relevance because of their wide application in industry and basic research. Appearance, according to the International Commission on Illumination,[1] is the visual sensation through which an object is perceived to have attributes such as size, shape, color, texture, gloss, transparency, opacity, etc. The specification of many correlates of visual attributes needs to be investigated yet, and this task requires the availability of goniospectrophotometric measurements of materials.

The goniospectrophotometer GEFE designed and developed at IO–CSIC was conceived to measure the spectral Bidirectional Reflectance Distribution Function (BRDF) at any pair of irradiation and detection directions, including out–of-plane and actual retro–reflection geometries.[2] The object of this instrument, as other similar goniospectrophotometers recently developed,[2–11] was to give support to the measurement of appearance, and its capabilities have allowed our research group to study thoroughly the geometrical and spectral scattering of a wide range of materials, from ceramic[12] to the quite complex special effect coatings,[13–18] whose color changes in a great extent at different irradiation/detection geometries; but also some characteristics of the diffuse reflectance standards: their spectral variation with the measurement geometry[19] and their retro–reflectance.[20]

Although the potential of this instrument has largely been proved, it still required to be upgraded to deal with some important scattering features for the assessment of the appearance. Since it was not provided with a detector with spatial resolution, it simply could not measure spectrophotometric quantites to characterize texture through the Bidirectional Texture Function[21] (BTF) or translucency through the more complex Bidirectional Scattering–Surface Reflectance Distribution Function[22] (BSSRDF). Sparkle, a sophisticated visual effect

Further author information:
Berta Bernad: E-mail: berta.bernad@csic.es
Alejandro Ferrero: E-mail: alejandro.ferrero@csic.es

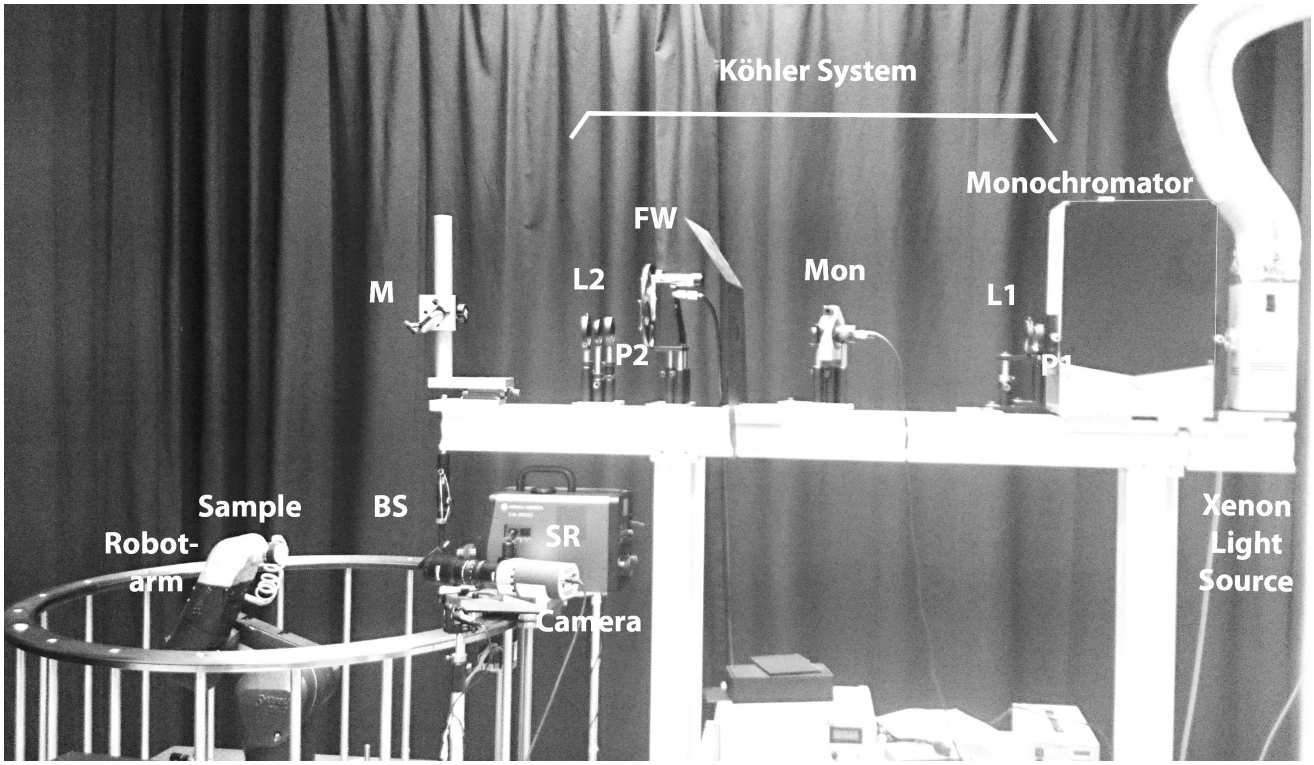

Figure 1. Picture of the goniospectrophotometer GEFE. L1: first converging lens; P1: diaphragm 1; L2: second converging lens; P2: diaphragm 2; Mon: monitor; FW: filter wheel; M: fold mirror; BS: beamsplitter; and SR: spectrorradiometer.

promoted by automotive industry[23] among other, and graininess are complex textures in which we are particularly interested. Sparkle highly depends on the irradiation/detection geometry but, when it is produced by interference pigments, also depends on the wavelength. Therefore, to accomplish our aim, GEFE needed to be upgraded with a detection system with spectral and spatial resolution.

Another requirement in the GEFE upgrading was to provide it with the capability of measuring fluorescence at different geometries, since some of the new pigments used in industry are fluorescent, which may have a non–negligible impact in the color of the product. Then, spectral resolution at irradiation and detection had to be available in GEFE.

This paper describes the upgrading of the goniospectrophotometer GEFE, and its new capabilities through the presentation of sparkle and goniofluorescence measurements. In addition, the potential of the instrument to evaluate translucency by the measurement of the BSSRDF will be briefly discussed.

2. DESCRIPTION OF THE GONIOSPECTROPHOTOMETER GEFE

As previously described at [Rabal et al. 2012],[2] GEFE (Fig. 1) comprises three systems: the irradiation one, the sample's positioning one and the detection system. The first one is fixed, whereas the other two systems are mobile: The sample is placed with the required orientation relative to the incoming beam, while the detector is attached to a cogwheel so as to be able to revolve around the sample. This arrangement permits a fast and accurate sampling.

2.1 Irradiation system

Though this design allows different types of light sources to be used, including narrow band spectral sources such as LEDs or lasers, to date GEFE had only been operated with a wide–band xenon lamp, which emits in

the 185 nm to 2000 nm spectral range. It was chosen because of its particularly high power emission in the short-wavelength range, which is the region where the spectroradiometer's response is smallest.

In order to irradiate uniformly and with a collimated beam the specimens, a Köhler optical system was used (see Fig. 1). It was formed by two 2-inch-diameter converging lenses (L1 and L2) made of UV Fused Silica and having a focal length of 75 mm and 500 mm, respectively. The distance between L1 and L2 is 88 cm. A diaphragm (P1) was placed after the first lens, which allows, by adjusting its diameter, the spot size on the sample to be modified, since it is precisely the image of P1. A second diaphragm (P2) is located after the second lens L2. By modifying its diameter, the irradiation solid angle is adjusted, but also the irradiation on the sample plane varies. This plane is located at a distance of 113 cm from L2. Between L1 and L2 there is a neutral-density-filter wheel (FW), used to produce different irradiance levels on the sample, depending on the particular measurement conditions. Before the filter wheel, an uncoated plate of fused silica redirects 10 % of the incoming beam towards a photodiode (Mon), whose role is monitoring the source's intensity. After the Köhler system, a mirror (M) was placed at 45°, followed by a 50:50 UV fused-silica broadband-plate beamsplitter (BS), also at 45° (see Fig. 1). This periscopic configuration makes it possible to perform retro-reflection measurements by placing the spectroradiometer (SR) behind the beamsplitter.

This system was upgraded with an optional monochromator to provide the irradiation with spectral resolution. It is a 300 mm focal length single monochromator in a Czerny-Turner configuration (TMc300, Bentham Instruments Ltd), with two diffraction gratings, one of 1200 g/mm (250 nm - 1200 nm), and other of 830 g/mm (500 nm - 1800 nm). It was located between the source and L1, by moving back the source (see Fig. 1).

2.2 Sample's positioning system

A six-axis robot-arm positions the sample quickly at the desired direction. The specimens are held by the robot-arm by means of a vacuum sucker. To date the robot-arm has only been operated for in– and out–of–plane BRDF measurements. The measurement of the Bidirectional Transmittance Distribution Function (BTDF) requires a separation between the robot-arm and the specimens to avoid occlusion of the transmitted light. Although the programming of the BTDF measurement procedure within the incident plane is solved, out–of–plane measurements are still a challenge, because the separation between the robot-arm and the specimens makes harder that the robot-arm reaches some positions.

2.3 Detection system

A spectroradiometer Konica-Minolta CS-2000 A is used to measure spectral radiance in the visible range (380 nm - 780 nm), with a variable field of view of 0.1°, 0.2° or 1°. This instrument is mounted onto a platform that travels along a 1.03 m diameter cogwheel, whose center coincides with the location of the sample's reference system. The movement along the cogwheel is performed by means of a stepper motor with a step coder for position control.

The system was upgraded with a CCD camera (Qimaging, Rollera XR) as detector to provide the acquisitions with spatial resolution, which is crucial for BTF and BSSRDF measurements. The dynamic range of the camera is 12 bits, the detector size is 695×520 pixels (2/3") and the pixel size 12.9 μm $\times$ 12.9 μm. Two objective lenses are available for the camera: An AF NIKKOR 50mm f/1.8D objective lens and a Navitar Zoom 7000 18:108 mm objective zoom lens. At the working distance, the field-of-view pixel area can be selected in the range between 50 μm $\times$ 50 μm and 130 μm $\times$ 130 μm.

2.4 Uniformity and angular distribution of irradiation

The bidirectional quantities used to describe scattering are defined for an infinitesimal area and perfectly specified directions. In practice, since physical apertures are finite, the evaluated area has a certain extension and the realized directions are composed by directions contained in cones with finite vertex angle. To understand properly the limitations of a bidirectional measurement, the equivalence between the theoretical definition and the expected result using real experimental conditions needs to be assessed.

On one hand, the finite size of the evaluated surface imposes two limitations: first, it broadens the distribution of directions from which light is collected; second, different areas are evaluated at different detection angles. As

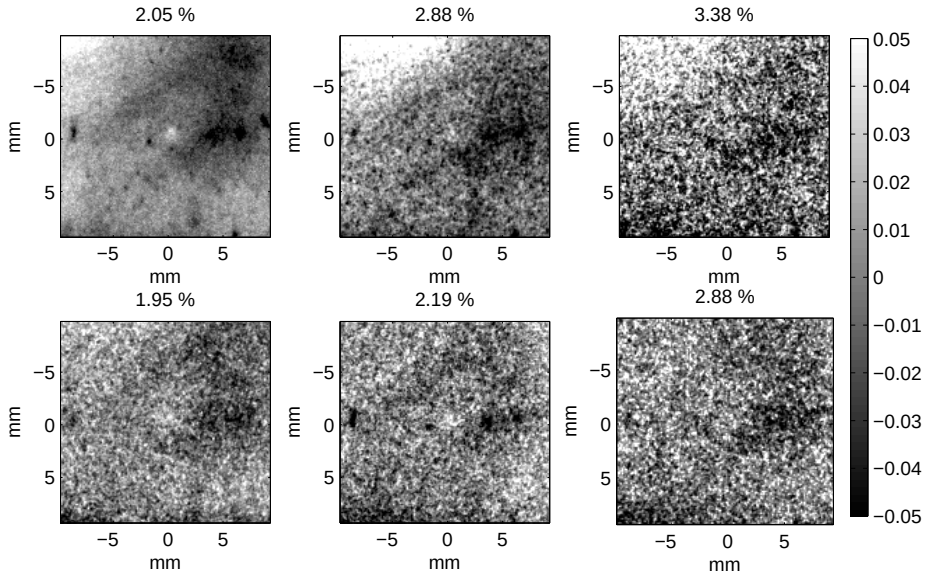

Figure 2. Images of irradiation on six different matt ceramic samples covering an area of 17 mm × 17 mm. Standard deviation of pixels is shown in percentage over the picture. On the right side the relative scale of response change is shown.

long as the specimen surface is uniform, this last limitation is not a problem when the detector is underfilled, because all scattered light is collected. However, when the detector is overfilled, the largest evaluated area needs to be uniformly irradiated to avoid considering different irradiances at different measurement geometries.

On the other hand, the broader the angular distribution of the irradiation, the more uncertainty we will had in the measurement, simply because at some point it is not possible to say whether the observed distribution is mainly produced by the surface or it prevails the distribution of the irradiation. This limitation is met around the specular directions of glossy surfaces.

These two important characteristics of the goniospectrophotometer, irradiation uniformity and angular distribution of the irradiation, can be studied in detail now by using the imaging system. Images of irradiation on six different matt ceramic standards are shown in Fig. 2, for an area of 17 mm × 17 mm. The relative uniformity, expressed on the top of each image, is sample-dependent and lies between 1.94 % and 3.38 %. It includes the non–uniformity of the sample, the non–uniformity of the irradiation and the non–uniformity of the camera.

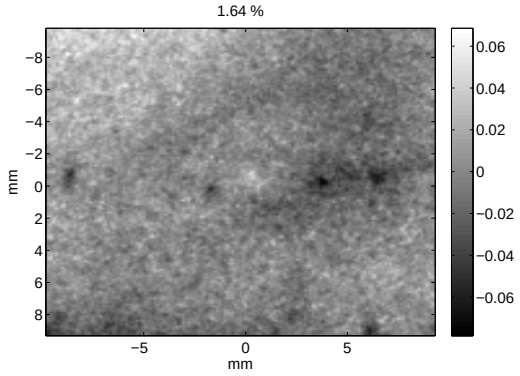

Figure 3. Average of the six images from Fig. 2, which mostly contains the non–uniformity of the irradiation and the non-uniformity of the camera.

By averaging the six images, a single image is obtained which mostly contains the non–uniformity of the irradiation and the non-uniformity of the camera (see Fig. 3), since their effects in the values of the pixels are correlated in the six images. The image has a standard deviation of 1.64 %, and this result shows that the uniformity of the irradiation in GEFE is high enough to assess typical non–uniformity in sample reflectance above shown. This image, obtained from images of different samples, would allow these experimental non–uniformities to be corrected by pixel-by-pixel division and to evaluate only that of the sample. Uniformity images as those shown in Fig. 2 should be used to estimate the average relative irradiance within the field-of-view area at every geometry, and to estimate the contribution to the uncertainty due to its variation. The more pixels integrated within the field-of-view area, the lower is the impact of the high spatial frequency fluctuations, but the larger the evaluated area, as in the case of high detection angles, the higher is the impact of low spatial frequency fluctuations.

By locating the CCD sensor of the camera on the focal plane of the objective lens, light from different directions will be detected by different pixels. This camera configuration allows the angular distribution of the incoming light to be evaluated. The evaluation was carried out for the irradiation beam, with an aperture stop 2 mm in diameter at lens L2. The result is shown on the left picture in Fig. 4. From the picture, it can be said that most of the incoming light is uniformly distributed in directions with angular deviations $\Delta\theta$ of $\pm 0.04^{o}$. This value limits the angular resolution of our system, unless smaller apertures are used. Although it is a good resolution to study the BRDF of glossy surfaces, it is not good enough to measure the BRDF of a mirror, as can be observed at the right picture in Fig. 4, which represents the angular distribution of the incoming light after reflection at a flat mirror. This is an almost identical picture to that obtained without mirror, but inverted by the mirror.

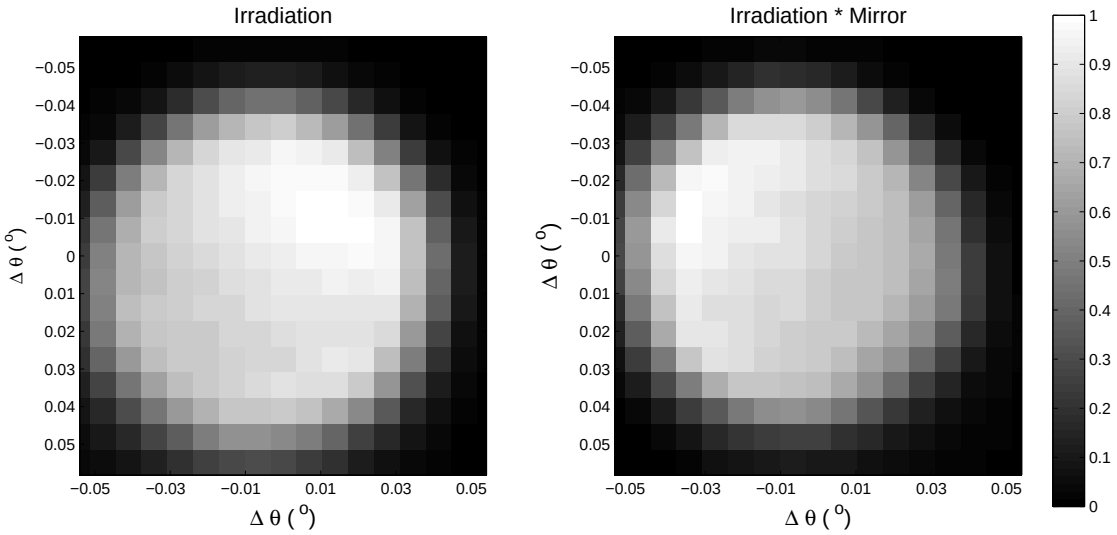

Figure 4. Angular distribution of light in the irradiation beam: incident beam (left) and after reflection at a flat mirror (right).

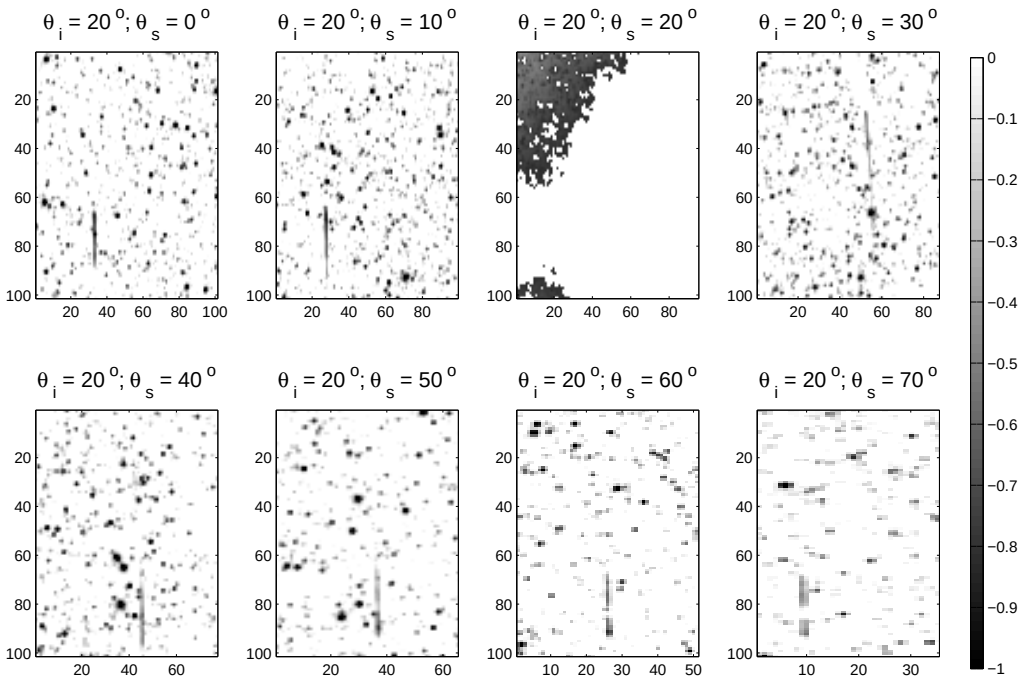

Figure 5. Eight experimental high–dynamic–range sparkle images corresponding with geometries with a fixed irradiation angle $\theta_{\rm i} = 20^{\rm o}$ and different detection angles $\theta_{\rm s}$ within the specular half-plane. A realtive log scale of the response is shown on the right side. Level 0 corresponds to the sample's background.

3. EXAMPLES OF PERFORMANCE

3.1 Near–field measurements: sparkle

A BASF coating with sparkle effect was visually selected to evaluate the dependence of sparkle on the irradiation and detection directions. Sample's images were acquired at measurement geometries resulting from combining irradiation angles respect to the coating normal ($\theta_{\rm i}$) from $0^{\rm o}$ to $70^{\rm o}$ (with angular steps of $10^{\rm o}$) and detection angles ($\theta_{\rm s}$) from $0^{\rm o}$ to $70^{\rm o}$ (with angular steps of $10^{\rm o}$ too), always within the incident plane. The field-of-view area of the pixels in the sample was estimated as 130 μm $\times$ 130 μm.

Eight experimental high–dynamic–range sparkle images are displayed in Fig. 5, which are representative of the kind of result that we obtain with our system. They correspond with geometries with a fixed irradiation angle $\theta_{\rm i} = 20^{\rm o}$ and different detection angles $\theta_{\rm s}$ within the specular half-plane. Image were scaled to highlight the density of the sparkle spots instead of the intensity. The values are in a logarithmic scale. The scale code is in inverted gray. It can be observed that the density of the sparkle spots decreases at higher aspecular angles (angular deviation between specular and detection directions). At the specular geometry ($\theta_{\rm i} = 20^{\rm o}$, $\theta_{\rm s} = 20^{\rm o}$), specular reflection on the clear coat prevails and just a saturated image is shown.

A more complete description of the sparkle measurement and these results can be found at reference [Ferrero et al. 2015].[24]

3.2 Goniofluorescence measurements

The variation of the fluorescence with the irradiation/detection geometry was assessed for a Spectralon fluorescence standard, which contains inorganic fluors. The relevant quantity to be measured was called Bidirectional Luminiscent Distribution Function (BLDF), which is calculated as the quotient of the luminiscent radiance for

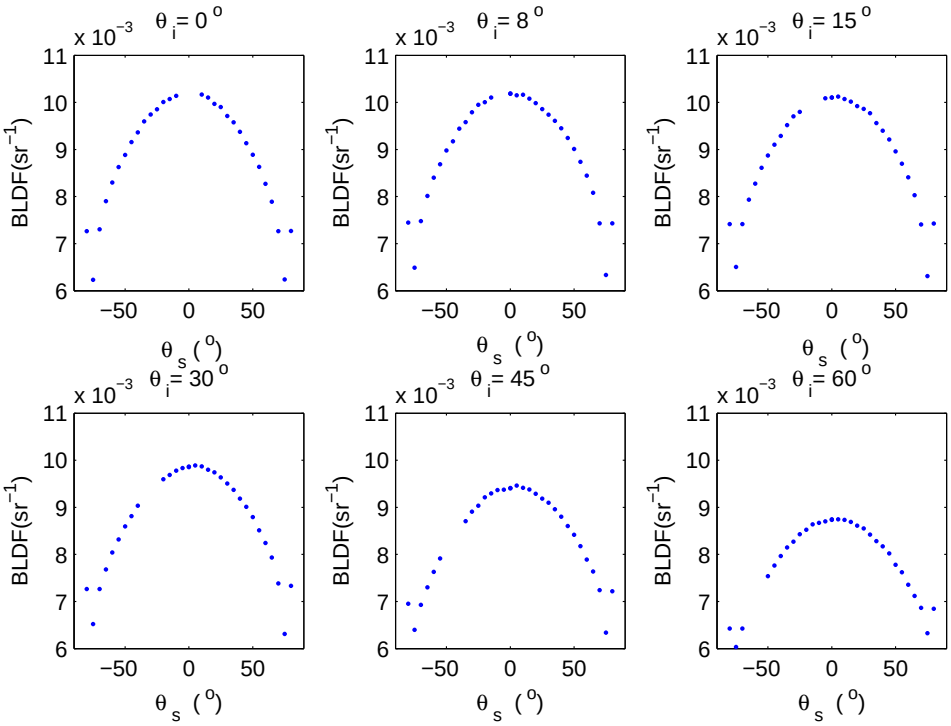

Figure 6. Goniofluorescence measurements of a Spectralon fluorescence standard. The figure represents the value of the BLDF at the wavelength of maximum fluorescence ($BLDF_{max}$) for every measurement geometry with an excitation wavelength of 380 nm. Incidence angle is shown over every graph.

a given detection direction and the irradiance on the surface from a given irradiation direction. It depends on the irradiation and detection directions and on the excitation and emission wavelengths.

The BLDF was measured for six irradiation polar angles ($\theta_i = 0^o$, 8°, 15°, 30°, 45° and 60°), with detection angles from $\theta_s = -80^o$ to $\theta_s = 80^o$ within the incident plane. It has to be noticed that, in this case, negative values of θ_s represent detection directions within the half incident plane containing irradiation direction, being positive otherwise. The results with an excitation wavelength of 380 nm are shown in Fig. 6. This figure represents the value of the BLDF at the wavelength of maximum fluorescence ($BLDF_{max}$, at 458 nm) for every measurement geometry. It has to be born in mind that, for this standard, the value of the BLDF at the excitation wavelength is almost $1/\pi$ sr^{-1}, which is the value of the BRDF of a perfectly reflecting diffuser (PRD).

It is observed that the variation of the $BLDF_{max}$ with respect to θ_s is very similar for all irradiation directions, with symmetrical decrease respect to $\theta_s = 0^o$. The same behavior was found for other excitation wavelengths (from 380 nm to 500 nm), and also for other four different Spectralon fluorescence standards.

3.3 Towards the measurement of BSSRDF: translucency

When an elementary surface of a translucent material is irradiated, part of the radiant flux penetrates inside the material. After subsurface scattering, a portion of radiant flux emerges from other different elementary surface, with specific angular distribution. The distribution function that describes this scattered flux is called Bidirectional Scattering–Surface Reflectance Distribution Function[22] (BSSRDF), and it needs to be measured to characterize translucency.[25,26] In general, the BSSRDF depends on the wavelength, on the spatial distribution of the scattered flux and on the irradiation/detection geometry.[27,28] A system able to modify the irradiation/detection geometry should be very valuable to characterize not only isotropic subsurface scattering, but also low order scattering, that is, when light only scatters few times before emerging.[28] The upgraded GEFE is completely prepared to accomplish the measurement of the BSSRDF, since it can deal with angular, spatial and

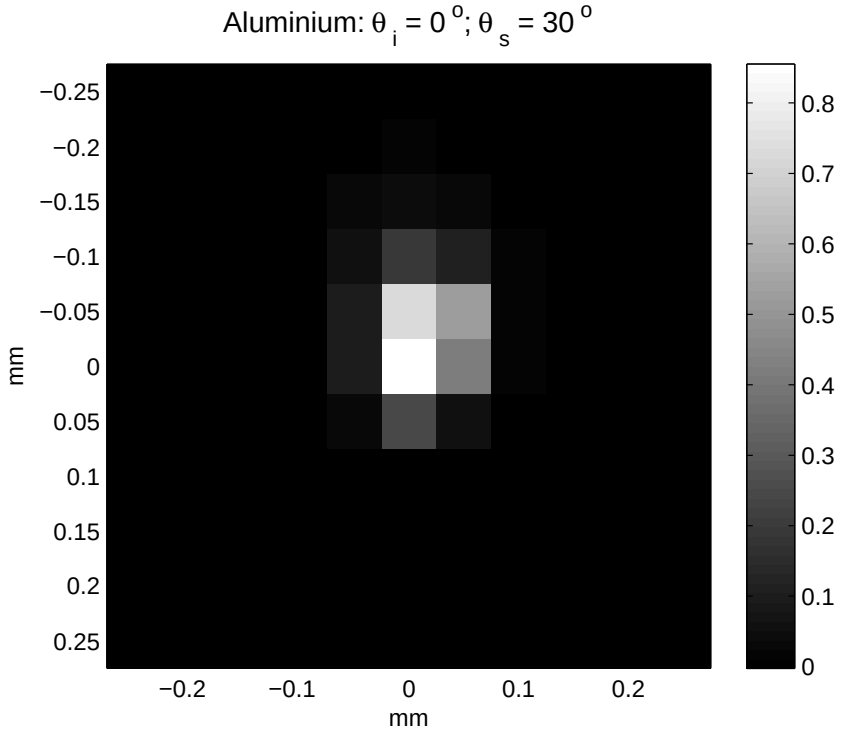

Figure 7. Image produced by using a 50 μm-diameter pinhole at L1 on an aluminium surface at $\theta_{\rm i} = 0^{\rm o}$ and $\theta_{\rm s} = 30^{\rm o}$, and with a a wavelength of 500 nm. Response scale is shown on the right side.

spectral distributions. One important issue to be addressed is the spatial resolution of our system for BSSRDF measurements. At maximum optical zoom, the pixel's field–of–view at our working distance is 50 μm $\times$ 50 μm, which is around four times higher than the human eye resolution (0.2 mm). However, the most important restriction of the BSSRDF resolution may be the size of the irradiation spot on the surface. A preliminary result was obtained by locating a 50 μm-diameter pinhole in front of L1. By considering only the magnification of the optical system, the image of the pinhole on the surface should occupy a circle of less than two pixels of diameter. The image measured by the camera using an aluminium surface as the irradiated surface (out of specular reflection) is of the size and shape shown in Fig. 7, resulting in an estimated FWHM of around 2 pixels (100 μm). The size of the spot is $1/\cos\theta_{\rm i}$ times bigger for the horizontal direction when $\theta_{\rm i}$ is not null.

To visually show the capabilities and limitations of our system to study the BSSRDF, translucency images of aluminium, soap and wax were acquired at the non-specular geometry [$\theta_{\rm i} = 0^{\rm o}$, $\theta_{\rm s} = 30^{\rm o}$]. The pixel's response [in digital numbers or DN divided by integration time (ms)] of the row containing the maximum of the irradiation spot is shown in Fig. 8, in a semi-logarithmic plot, as a function of the distance to the maximum. Whereas in the case of aluminium any appreciable response is observed in non-irradiated pixels, in the case of wax and soap, very clear tails are observed on the left of the irradiation spot. The tails are characteristics of translucent materials,[25,26] and they can be featured by GEFE, as it is shown in this preliminary study.

4. CONCLUSIONS

The gonio–spectrophotometer GEFE designed and developed at IO-CSIC, conceived to measure the spectral Bidirectional Reflectance Distribution Function (BRDF) at any pair of irradiation and detection directions, has been upgraded to extend its capabilities. On one hand, a camera has been integrated in the instrument to allow near–field measurements to be carried out. This new feature is crucial to characterize texture through the Bidirectional Texture Function[21] (BTF) or translucency through the more complex Bidirectional Scattering–Surface

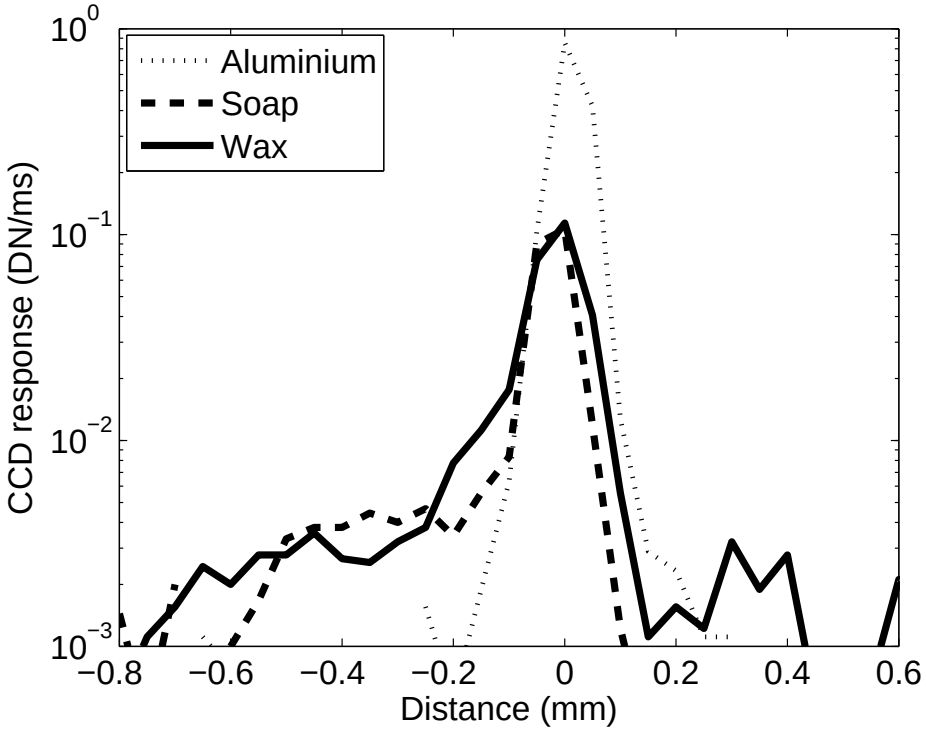

Figure 8. CCD row response to a spot irradiating a sample of aluminium, soap and wax ($\theta_i = 0^o$ and $\theta_s = 30^o$).

Reflectance Distribution Function (BSSRDF). In addition, the camera permits to evaluate important characteristics of the irradiation on the sample, namely its uniformity and its angular distribution. On the other hand, a monochromator has been located in front of the source to obtain spectral resolution at irradiation, which not only permits to provide with spectral resolution the near–field measurements, but also to carry out the dependence of the fluorescence on the irradiation and detection directions, or goniofluorescence. Goniofluorescence and sparke measurements have been shown as examples of the performance of the upgraded gonio–spectrophotometer. Finally, its capability to measure BSSRDF have been briefly discussed.

ACKNOWLEDGMENTS

Authors are grateful to EMRP for funding the project "Multidimensional reflectometry for industry". The EMRP is jointly funded by the EMRP participating countries within EURAMET and the European Union. Authors are also grateful to Comunidad de Madrid for funding the project SINFOTON-CM: S2013/MIT-2790.

REFERENCES

[1] Pointer, M., "CIE publication 175-2006: CIE TC1-65 Technical Report," in [*A Framework for the Measurement of Visual Appearance*], CIE (2006).

[2] Rabal, A. M., Ferrero, A., Campos, J., Fontecha, J. L., Pons, A., Rubiño, A. M., and Corróns, A., "Automatic gonio-spectrophotometer for the absolute measurement of the spectral brdf at in-and out-of-plane and retroreflection geometries," *Metrologia* **49**, 213–223 (2012).

[3] Obein, G., Bousquet, R., and Nadal, M. E., "New NIST reference goniospectrometer," *Proc. SPIE* **5880**, 241–250 (2005).

[4] Germer, T. A. and Asmail, C. C., "Goniometric optical scatter instrument for out-of-plane ellipsometry measurements," *Rev. Sci. Instrum.* **70**, 3688–3695 (1999).

[5] Hünerhoff, D., Grusemann, U., and Höpe, A., "New robot-based gonioreflectometer for measuring spectral diffuse reflection," *Metrologia* **43**, S11–S16 (2006).

[6] Leloup, F. B., Forment, S., Dutré, P., Pointer, M. R., and Hanselaer, P., "Design of an instrument for measuring the spectral bidirectional scatter distribution function," *Appl. Opt.* **47**, 5454–5467 (2008).

[7] Baribeau, R., Neil, W. S., and Côté, E., "Development of a robot-based gonioreflectometer for spectral brdf measurement," *Journal of Modern Optics* **56**, 1497–1503 (2009).

[8] Nevas, S., Manoocheri, F., and Ikonen, E., "Gonioreflectometer for measuring spectral diffuse reflectance," *Appl. Opt.* **43**, 6391–6399 (2004).

[9] Matsapey, N., Faucheu, J., Flury, M., and Delafosse, D., "Design of a gonio-spectrophotometer for optical characterization of gonio–apparent materials," *Meas. Sci.Technol.* **24**, 065901 (2013).

[10] Ouarets, S., Ged, G., Razet, A., and Obein, G., "A new gonioreflectometer for the measurement of the bidirectional reflectance distribution function (brdf) at lne-cnam," *Proceedings of CIE 2012 "Lighting Quality and energy efficiency"* **5880**, 687–691 (2012).

[11] Patrick, H. J., Zarobila, C. J., and Germer, T. A., "The NIST robotic optical scatter instrument (ROSI) and its application to brdf measurements of diffuse reflectance standards for remote sensing," *SPIE Optical Engineering+Applications. International Society for Optics and Photonics*, 886615–886615–12 (2013).

[12] Ferrero, A., Campos, J., Rabal, A. M., Pons, A., Hernanz, M. L., and Corróns, A., "Principal components analysis on the spectral bidirectional reflectance distribution function of ceramic colour standards," *Journal of the Optical Society of America A* **20**, 19199–19211 (2011).

[13] Ferrero, A., Rabal, A. M., Campos, J., Pons, A., and Hernanz, M. L., "Variables separation of the spectral BRDF for better understanding color variation in special effect pigment coatings," *Journal of the Optical Society of America A* **29**, 842–847 (2012).

[14] Ferrero, A., Rabal, A. M., Campos, J., Martínez-Verdú, F., Chorro, E., Perales, E., Pons, A., and Hernanz, M. L., "Spectral BRDF-based determination of proper measurement geometries to characterize color shift of special effect coatings," *Journal of the Optical Society of America A* **30**, 206–214 (2013).

[15] Kirchner, E. and Ferrero, A., "Isochromatic lines as extension of the Helmholtz reciprocity principle for effect paints," *Journal of the Optical Society of America A* **31**, 1861–1867 (2014).

[16] Ferrero, A., Perales, E., Rabal, A. M., Campos, J., Martínez-Verdú, F. M., Chorro, E., and Pons, A., "Color representation and interpretation of special effect coatings," *Journal of the Optical Society of America A* **31**, 436–447 (2014).

[17] Ferrero, A., Bernad, B., Campos, J., Martínez-Verdú, F. M., Perales, E., van der Lans, I., and Kirchner, E., "Towards a better understanding of the color shift of effect coatings by densely sampled spectral BRDF measurement," *Proc. SPIE 9018, Measuring, Modeling, and Reproducing Material Appearance*, 90180K (2014).

[18] Ferrero, A., Campos, J., Perales, E., Martínez-Verdú, F. M., van der Lans, I., and Kirchner, E., "Global color estimation of special-effect coatings from measurements by commercially available portable multiangle spectrophotometers," *Journal of the Optical Society of America A* **32**, 1–11 (2015).

[19] Ferrero, A., Rabal, A. M., Campos, J., Pons, A., and Hernanz, M. L., "Spectral and geometrical variation of the bidirectional reflectance distribution function of diffuse reflectance standards," *Applied Optics* **51**, 8535–8540 (2012).

[20] Rabal, A. M., Ferrero, A., Campos, J., Pons, A., and Hernanz, M. L., "Bidirectional reflectance distribution function of diffuse reflectance standards around the retro–reflection direction," *Metrologia* **51**, 148–153 (2014).

[21] K. J. Dana, B. van Ginneken, S. K. N. and Koenderink, J. J., "Reflectance and texture of real-world surfaces," *ACM Transactions on Graphics (TOG)* **18**, 1–34 (1999).

[22] Nicodemus, F. E., Richmond, J. C., and Hsia, J. J., [*Geometrical considerations and nomenclature for reflectance*], Natl. Bur. Stand. Monogr. **160** (1977).

[23] Kirchner, E., van den Kieboom, G. J., Njo, L., Sùper, R., and Gottenbos, R., "Observation of visual texture of metallic and pearlescent materials," *Col. Res. Appl.* **32**, 256–266 (2007).

[24] Ferrero, A. and Bayón, S., "The measurement of sparkle," *Metrologia* (Submitted, 2015).

[25] Inoshita, C., Tagawa, S., Mannan, M. A., Mukaigawa, Y., and Yagi, Y., "Full-dimensional sampling and analysis of BSSRDF," *IPSJ Transactions on Computer Vision and Applications* **5(0)**, 119–123 (2013).

[26] Gkioulekas, I., Zhao, S., Bala, K., Zickler, T., and Levin, A., "Inverse volume rendering with material dictionaries," *ACM Transaction on Graphics (Proc. ACM SIGGRAPH Asia)* (2013).

[27] Jensen, H. W., Marschner, S. R., Levoy, M., and Hanrahan, P., "A practical model for subsurface light transport," *Proceedings of the 28th annual conference on Computer graphics and interactive techniques*, 511–518 (2001).

[28] Donner, C., Lawrence, J., Ramamoorthi, R., Hachisuka, T., Jensen, H. W., and Nayar, S., "An empirical BSSRDF model," *ACM Trans. Graph.* **28**, 30:1–30:10 (July 2009).